Uncovering the critical soil moisture thresholds of plant water stress for European ecosystems

Author(s):
Fu, Zheng; Ciais, Philippe; Makowski, David; Bastos, Ana; Stoy, Paul C.; Ibrom, Andreas; Knohl, Alexander; Migliavacca, Mirco; Cuntz, Matthias; Šigut, Ladislav; Peichl, Matthias; Loustau, Denis; El-Madany, Tarek S.; Buchmann, Nina; Gharun, Mana; Janssens, Ivan; Markwitz, Christian; Grünwald, Thomas; Rebmann, Corinna; Mölder, Meelis; Varlagin, Andrej; Mammarella, Ivan; Kolari, Pasi; Bernhofer, Christian; Heliasz, Michal; Vincke, Caroline; Pitacco, Andrea; Cremonese, Edoardo; Foltýnová, Lenka; Wigneron, Jean-Pierre

Publication date:
2022-03

Permanent link:
https://doi.org/10.3929/ethz-b-000522368

Originally published in:
Global Change Biology 28(6), https://doi.org/10.1111/gcb.16050

Uncovering the critical soil moisture thresholds of plant water stress for European ecosystems

Fu, Zheng; Ciais, Philippe; Makowski, David; Bastos, Ana; Stoy, Paul C.; Ibrom, Andreas; Knohl, Alexander; Migliavacca, Mirco; Cuntz, Matthias; Šigut, Ladislav

Total number of authors:
30

Published in:
Global Change Biology

Link to article, DOI:
10.1111/gcb.16050

Publication date:
2022

Document Version
Peer reviewed version

DR. ZHENG FU (Orcid ID : 0000-0001-7627-8824)
DR. ANA BASTOS (Orcid ID : 0000-0002-7368-7806)
DR. LADISLAV ŠIGUT (Orcid ID : 0000-0003-1951-4100)
DR. MATTHIAS PEICHL (Orcid ID : 0000-0002-9940-5846)
DR. TAREK S. EL-MADANY (Orcid ID : 0000-0002-0726-7141)

Article type : Research Article

Uncovering the critical soil moisture thresholds of plant water stress for European ecosystems

Running title: Critical soil moisture thresholds in Europe

Article type: Primary Research Articles

Zheng Fu[1*], Philippe Ciais[1], David Makowski[2], Ana Bastos[3], Paul C. Stoy[4], Andreas Ibrom[5], Alexander Knohl[6], Mirco Migliavacca[3], Matthias Cuntz[7], Ladislav Šigut[8], Matthias Peichl[9], Denis Loustau[10], Tarek S. El-Madany[3], Nina Buchmann[11], Mana Gharun[11], Ivan Janssens[12], Christian Markwitz[6], Thomas Grünwald[13], Corinna Rebmann[14], Meelis Mölder[15], Andrej Varlagin[16], Ivan Mammarella[17], Pasi Kolari[17], Christian Bernhofer[13], Michal Heliasz[18], Caroline Vincke[19], Andrea Pitacco[20], Edoardo Cremonese[21], Lenka Foltýnová[8], Jean-Pierre Wigneron[10]

Zheng Fu: https://orcid.org/0000-0001-7627-8824
Philippe Ciais: https://orcid.org/0000-0001-8560-4943
Ana Bastos: https://orcid.org/0000-0002-7368-7806
Paul C. Stoy: https://orcid.org/0000-0002-6053-6232
Andreas Ibrom: https://orcid.org/0000-0002-1341-921X
Alexander Knohl: https://orcid.org/0000-0002-7615-8870
Mirco Migliavacca: https://orcid.org/0000-0003-3546-8407
Matthias Cuntz: https://orcid.org/0000-0002-5966-1829
Ladislav Šigut: https://orcid.org/0000-0003-1951-4100
Matthias Peichl: https://orcid.org/0000-0002-9940-5846
Tarek S. El-Madany: https://orcid.org/0000-0002-0726-7141
Nina Buchmann: https://orcid.org/0000-0003-0826-2980
Mana Gharun: https://orcid.org/0000-0003-0337-7367
Ivan Janssens: https://orcid.org/0000-0002-5705-1787
Thomas Grünwald: https://orcid.org/0000-0003-2263-0073
Corinna Rebmann: https://orcid.org/0000-0002-8665-0375
Andrej Varlagin: https://orcid.org/0000-0002-2549-5236
Ivan Mammarella: https://orcid.org/0000-0002-8516-3356
Christian Bernhofer: https://orcid.org/0000-0003-1061-3073
Michal Heliasz: https://orcid.org/0000-0003-2635-9604
Andrea Pitacco: https://orcid.org/0000-0002-7260-6242
Jean-Pierre Wigneron: https://orcid.org/0000-0001-5345-3618

[1] Laboratoire des Sciences du Climat et de l'Environnement, LSCE/IPSL, CEA-CNRS-UVSQ, Université Paris-Saclay, Gif-sur-Yvette, 91191, France
[2] Unit Applied mathematics and computer science (UMR 518) INRAE AgroParisTech Université Paris-Saclay, Paris, France

[3] Department Biogeochemical Integration, Max Planck Institute for Biogeochemistry, D-07745 Jena, Germany
[4] Department of Biological Systems Engineering, University of Wisconsin – Madison, USA
[5] Technical University of Denmark, Department of Environmental Engineering, Lyngby, Denmark
[6] University of Goettingen, Büsgenweg 2, 37077 Göttingen, Germany
[7] Université de Lorraine, AgroParisTech, INRAE, UMR Silva, 54000 Nancy, France
[8] Global Change Research Institute of the Czech Academy of Sciences, Bělidla 986/4a, CZ-60300 Brno, Czech Republic
[9] Department of Forest Ecology and Management, Swedish University of Agricultural Sciences, Skogsmarksgränd, 90183 Umeå, Sweden
[10] ISPA, Bordeaux Sciences Agro, INRAE, F-33140, Villenave d'Ornon, France
[11] Department of Environmental Systems Science, ETH Zurich, Universitaetstr. 2, 8092 Zurich, Switzerland
[12] Center of Excellence Global Change Ecology, Department of Biology, University of Antwerp, Universiteitsplein 1, Wilrijk, 2610 Belgium
[13] Faculty of Environmental Sciences, Institute of Hydrology and Meteorology, Technische Universit¨at Dresden, 01062, Germany
[14] Department Computational Hydrosystems, Helmholtz Centre for Environmental Research – UFZ
[15] Department of Physical Geography and Ecosystem Science, Lund University, Sölvegatan 12, SE-223 62 Lund, Sweden
[16] A.N. Severtsov Institute of Ecology and Evolution, Russian Academy of Sciences, 119071, Leninsky pr.33, Moscow, Russia
[17] Institute for Atmospheric and Earth System Research/Physics, Faculty of Science, University of Helsinki, Helsinki, Finland
[18] Centre for Environmental and Climate Research, Lund University, Lund, Sweden
[19] Earth and Life Institute - Environmental Sciences, Université catholique de Louvain

[20] University of Padova, DAFNAE, Viale dell'Università 16, I-35020 Legnaro, Italy

[21] Climate Change Unit, Environmental Protection Agency of Aosta Valley, Italy

*Correspondence to: zheng.fu@lsce.ipsl.fr

Abstract

Understanding the critical soil moisture (SM) threshold (θ_{crit}) of plant water stress and land surface energy partitioning is a basis to evaluate drought impacts and improve models for predicting future ecosystem condition and climate. Quantifying the θ_{crit} across biomes and climates is challenging because observations of surface energy fluxes and SM remain sparse. Here, we used the latest database of eddy covariance measurements to estimate θ_{crit} across Europe by evaluating evaporative fraction (EF)-SM relationships and investigating the covariance between vapor pressure deficit (VPD) and gross primary production (GPP) during SM dry-down periods. We found that the θ_{crit} and soil matric potential threshold in Europe are 16.5% and −0.7 MPa, respectively. Surface energy partitioning characteristics varied among different vegetation types; EF in savannas had the highest sensitivities to SM in water-limited stage, and the lowest in forests. The sign of the covariance between daily VPD and GPP consistently changed from positive to negative during dry-down across all sites when EF shifted from relatively high to low values. This sign of the covariance changed after longer period of SM decline in forests than in grasslands and savannas. Estimated θ_{crit} from the VPD-GPP covariance method match well with the EF-SM method, showing this covariance method can be used to detect the θ_{crit}. We further found that soil texture dominates the spatial variability of θ_{crit} while shortwave radiation and VPD are the major drivers in determining the spatial pattern of EF sensitivities. Our results highlight for the first time that the sign change of the covariance between daily VPD and GPP can be used as an indicator of how ecosystems transition from energy to SM limitation. We also characterized the corresponding θ_{crit} and its drivers across diverse ecosystems in Europe, an essential variable to improve the representation of water stress in land surface models.

Keywords: critical soil moisture threshold, surface energy partitioning, vapor pressure deficit, evaporative fraction, gross primary production, drought, Europe

1. Introduction

The critical soil moisture (SM) threshold of plant water stress is the point when evapotranspiration starts to decrease due to the SM deficit (Feldman *et al.*, 2019, Seneviratne *et al.*, 2010). Below this threshold, exhaustion of SM leads to reduced evapotranspiration and increased partitioning towards sensible heat flux due to higher surface temperatures that lead to drier air and an increase in the vapor pressure deficit (VPD), which impairs important ecosystem functions like carbon dioxide uptake (Betts, 2004, Gentine *et al.*, 2019, Granier *et al.*, 2007, Seneviratne *et al.*, 2010). SM therefore plays a crucial role in partitioning of available between latent and sensible heat fluxes from the land surface (Schwingshackl *et al.*, 2017). This energy partitioning determines local climate and influences the terrestrial component of land-atmosphere coupling (Santanello Jr *et al.*, 2018). Thus, it is imperative to quantify the critical SM thresholds (θ_{crit}) of plant water stress and surface energy partitioning characteristics for evaluating the drought impacts on ecosystem function and improving models to predict future climate accurately.

The evaporative fraction (EF) is the ratio of latent heat flux to the sum of latent and sensible heat fluxes, and EF-SM relationships are commonly used to quantify θ_{crit} and surface energy partitioning characteristics (Budyko, 1974, Koster *et al.*, 2009, Seneviratne *et al.*, 2010). SM directly limits evapotranspiration under SM-limited conditions, which increase surface temperature at a given level of net radiation, driving a positive land-atmosphere climate feedback (Betts, 2004, Gentine *et al.*, 2019, Seneviratne *et al.*, 2010). At higher SM availability, the system is considered energy limited as more moisture does not necessarily lead to greater evapotranspiration, and the strength of the water, carbon, and energy cycle coupling is subdued (Feldman *et al.*, 2019, Pendergrass *et al.*, 2020). Evapotranspiration is at or near its potential value where net radiation and atmospheric resistance are instead limiting. This EF-SM framework is well established (Fig. 1) but quantifying the θ_{crit} that determines the transition from energy to water-limited regimes across biomes and climates is challenging because surface energy fluxes and SM observations remain sparse (Baldocchi *et al.*, 2004,

Budyko, 1974, Feldman *et al.*, 2019, Koster *et al.*, 2009). The extreme drought events that help quantify θ_{crit} are, by definition, rare, and often require long observational time series.

Attempts have been made to characterize these different evapotranspiration regimes at sub-monthly scales using satellite greenness data and air temperature globally (Zscheischler *et al.*, 2015), for North America (Short Gianotti *et al.*, 2019), and on weekly scales for Africa using satellite remote sensing data of the diurnal amplitude of the land surface temperature and surface soil moisture (Feldman *et al.*, 2019). These studies did not investigate the role of VPD, but recently, both observations and models showed that VPD increases tend to reduce gross primary production (GPP) across a large range of SM conditions, whereas the reduction of SM only reduces GPP below a critical SM threshold (Green *et al.*, 2019, Grossiord *et al.*, 2020, Kimm *et al.*, 2020). GPP and evapotranspiration are tightly coupled on short time scales (Gentine *et al.*, 2019), and we argue that the sign of the covariance between daily VPD and GPP can be an indicator of the relative strength between the water and energy limitation on ecosystem function. This is because VPD combines the effects of both water and enthalpy (via temperature) on GPP (Grossiord *et al.*, 2020, Kimm *et al.*, 2020, Novick *et al.*, 2016). GPP is positively related to radiation under energy-limited regimes (Fig. 1), and positively correlated with SM under water-limited regimes (Gentine *et al.*, 2019, Seneviratne *et al.*, 2010). However, it is unknown if the sign change of covariance between daily VPD and GPP is also an effective metric to a describe surface energy partitioning characteristics between water- and energy-limited regimes, and *vice versa*.

The dry-down periods following rainfall, i.e., long periods without rainfalls when soil moisture decreases (Akbar *et al.*, 2018, Feldman *et al.*, 2018, Feldman *et al.*, 2019), provide a natural experiment for us to evaluate the EF-SM relationships and investigate how the sign of the covariance between daily VPD and GPP changes as SM declines and ecosystems shift from energy to water-limited states. During the course of a dry-down, an ecosystem with θ_{crit} will transition from a regime during which higher VPD is driven by incoming radiation which increases GPP, to another regime where SM reductions increase VPD but reduce GPP. During a SM dry-down, there is generally an initial period of GPP increase due to available SM after

rainfall if the ecosystem is already water limited before the dry-down counting started, and is followed by a decline (Fig. 1); but VPD keeps increasing if the incoming solar radiation (RAD) remains stable, e.g., in the presence of anticyclonic conditions (Feldman *et al.*, 2020). During the initial increasing GPP period, energy-limitation (e.g., photosynthetically active radiation or temperature) is the major driver of GPP while SM becomes a key limiting factor during the following GPP decreasing stage (Seneviratne *et al.*, 2010). However, the relationships between VPD and GPP in these two different stages may be different. We hypothesize that the covariance between daily VPD and GPP can be used to detect these two regimes during dry-downs, i.e., one regime with energy limiting conditions (positive covariance) and one regime with water limiting conditions (negative covariance).

During a dry-down, EF first remains constant but then decreases when SM becomes lower than a given threshold (Fig. 1). The EF–SM relationship is characterized by a transition point in SM separating the water and energy-limited regimes (Koster *et al.*, 2009, Seneviratne *et al.*, 2010). There is limited opportunity to test the appearance of SM limitations during dry episodes across a wide diversity of biomes and climates because EF–SM relationships are infrequently characterized due to the challenge of directly measuring surface energy fluxes and SM across sites (Baldocchi *et al.*, 2004, Budyko, 1974, Feldman *et al.*, 2019, Koster *et al.*, 2009). To our knowledge, there is no observation-based assessment of the transition point of SM between demand and soil water supply limitation across Europe. Even less is known about the controlling factors and mechanisms in determining the θ_{crit} across diverse ecosystems. Climate models, on the other hand, rely on a parametric representation of SM–evaporation relationships to describe associations between water and energy cycles and predict future climate. However, due to difficulty in observing EF at large scales to constrain model results, and the lack of model simulation output at daily or hourly time steps, these relationships take different forms across climate models which contribute to divergences and uncertainty in making climate projections (Dirmeyer *et al.*, 2006, Feldman *et al.*, 2019, Schwingshackl *et al.*, 2017).

The recently released ICOS (Integrated Carbon Observation System network of eddy covariance observations)(Centre, 2019) dataset with continuously measured CO_2, water vapor, and energy fluxes in Europe allows more direct observations of EF–SM relationships over various biomes and climates. Further, this dense network provides a unique opportunity to evaluate EF–SM relationships and change in the covariance between VPD and GPP during dry-downs. In recent years, Europe has experienced a series of extreme summer drought and heat events (e.g., 2003, 2010, 2015 and 2018), each characterized by record-breaking climate anomalies and extensive dry-down periods (Bastos *et al.*, 2020a, Bastos *et al.*, 2020b, Fu *et al.*, 2020). We can thus investigate the surface energy partitioning-SM relationship during these dry-downs (episodes with no rain for several consecutive days (Fig. 1)) where SM shows a short term rise after rain and then decreases until the next rain event. There were many 'dry-down' periods with no rain in Europe in recent years that can be used to detect the critical moisture value at the onset of water stress.

Focusing on SM dry-downs, this study uses the latest eddy covariance measurements from ICOS to quantify θ_{crit} across Europe and test the hypothesis that the sign change of covariance between daily VPD and GPP can be used to detect θ_{crit}. By evaluating the EF-SM relationships, we first quantify θ_{crit} values and the EF sensitivity to SM in the water-limited regime. Then, we investigate the changes of covariance between daily VPD and GPP during SM dry-downs and quantify θ_{crit} values with this second approach, which are compared with the θ_{crit} from the first approach. Last, we explore what factors drive the spatial variability of θ_{crit} and EF sensitivity to SM.

2. Materials and Methods

2.1 Datasets

We used half-hourly SM, VPD, GPP, precipitation, latent heat flux, sensible heat flux and incoming shortwave radiation from the recently released ICOS (Integrated Carbon Observation System) dataset (Centre, 2019). ICOS includes 52 eddy covariance sites in Europe with energy, water, carbon fluxes and meteorological data, which were processed

following a consistent and uniform processing pipeline (Pastorello *et al.*, 2020). We selected 31 sites with measurements for all above variables, including 22 forests, 5 grasslands, 3 savannas and 1 shrubland (Table S1). Savanna sites include both trees and grasses and in our case are found in Mediterranean climate zones (El-Madany *et al.*, 2020, Luo *et al.*, 2018, Luo *et al.*, 2020). Croplands were excluded due to the effect of management on the seasonal timing of ecosystem fluxes, both from crop rotations and from the varying timing of planting and harvesting. Wetland sites were also removed because they have a high water table and infrequently show soil moisture limitations.

SM was measured as volumetric soil water content (percentage) at different depths, varying across sites. Surface SM (SM_1: 0-5 cm) was measured at all sites and some sites also provided deeper SM measurements (e.g., SM_2: 5-20 cm; SM_3: 20-60 cm). We mainly used the surface SM observations but deeper SM measurements were also used when available. GPP estimates from the night-time partitioning method were used for the analysis (Reichstein *et al.*, 2005). Data were quality controlled so that only measured and good-quality gap filled data (QC = 0 or 1) were used. Daytime half-hourly data (9 am to 16 pm local standard time) were averaged to daily values while SM values were averaged over the full day.

Measured soil texture, mean annual precipitation, summer average of VPD, incoming shortwave radiation and wind speed data at each site were also used to understand the drivers in determining the spatial variability of θ_{crit} and EF sensitivity to SM in water-limited stage.

2.2 Soil moisture dry-down identification

Dry-downs following rainfall are episodes with no rain for several consecutive days during which SM shows a short term 'pulse' rise after rain and then decays until the next rain event. A dry-down is retained for our analysis when SM decreases consecutively for at least 10 days after rainfall (Akbar *et al.*, 2018, Feldman *et al.*, 2018, McColl *et al.*, 2017, Shellito *et al.*, 2018). Days with intermittent rainfall are excluded. We focused on the soil dry-downs during the summer (June−July−August) season for all available site-years. This resulted in 428 dry-down events that form the basis of our study.

2.3 Critical SM threshold and evaporative fraction sensitivity to SM estimation

We calculated the daily evaporative fraction (EF) as the ratio of observed latent heat flux to the sum of latent and sensible heat fluxes during each soil dry-down. Then, we characterized the EF-SM relationship at each site using all available soil dry-downs, from a regression between these two variables with a linear-plus-plateau model:

$$EF = \begin{cases} a + b(SM - c) & if\ SM < \theta_{crit} \\ a & if\ SM \geq \theta_{crit} \end{cases}$$

where a is the maximum value of EF in absence of SM stress (energy-limited stage), b represents the slope of the linear increase phase (water-limited stage), and c is the critical SM threshold. These three parameters were simultaneously estimated by least squares fit with the R software package 'nlstools' (Baty *et al.*, 2015) for each site, leading to site-specific estimated values of peak EF, slope and θ_{crit}. θ_{crit} is the breakpoint until which EF increases linearly as a function of SM (Figs. 1 and S1). The slope represents the EF sensitivity to SM in the water-limited regime, indicating the magnitude of EF increase for each additional 1% change in SM when SM is below its breakpoint. The plateau is the maximum EF value reached when SM exceeds its threshold. The time spent in the water-limited stage was computed as the ratio of the number of days with SM<threshold divided by the total duration of the dry down as in Feldman *et al.* (2019). SM threshold values were converted to soil matric potentials using soil retention curves and soil texture data (Table S1) (Gourlez de la Motte *et al.*, 2020, Granier *et al.*, 2007, Marthews *et al.*, 2014).

There were 23, 16 and 12 sites with the critical SM threshold estimates based on the first (SM_1), second (SM_2), and third (SM_3) soil water content measurement depth (Figs. S1-3), respectively. For the rest of sites, it was not possible to estimate a SM threshold using the EF-SM relationship because samples were too infrequent, deep SM measurements were missing, or there were no thresholds.

2. 4 Covariance between daily VPD and GPP during dry-down

We also calculated the covariance between daily VPD and GPP across nine-day moving

windows during the dry-down (e.g., 1-9 days; 2-10 days; 3-11 days…). A positive covariance indicates that higher VPD is associated with increases of GPP (which we term 'radiation effects') while a negative covariance indicates that water stress limits GPP, i.e., with a higher VPD caused by dryer soils results in a lower GPP. Here, we excluded some short dry-downs because their covariances during the dry-down are all positive or negative, suggesting the entire dry-down period is under energy-limited or water-limited stage. We only chose the long soil dry-downs with at least 15 days (with at least 7 covariance values) and their covariances must include both positive and negative values to see if the change of covariance signs corresponds to the ecosystem transition from energy-limited into water-limited regime.

The evolution of covariance with moving window days during the dry-down periods allowed us to evaluate the joint variability of daily VPD and GPP change. Across all soil dry-downs, the median value of the VPD-GPP covariance was calculated for equal bins of 1 day change to identify the timing when the sign of covariance will change. Similar to the covariance, the average of SM during the moving window (e.g., 1-9 days; 2-10 days; 3-11 days…) were also calculated to detect the critical SM threshold when the sign of covariance changes. The correlation of Pearson and Spearman and their associated test were performed to compare the θ_{crit} values from this covariance method with the EF-SM method.

2.5 Drivers of the spatial variability of critical SM thresholds and EF slopes

We evaluated the relative importance of soil texture, mean annual precipitation, summer average VPD, incoming shortwave radiation and wind speed in determining the spatial variability of θ_{crit} and EF sensitivities to SM. We used a relative importance analysis approach to quantify the relative contributions of each factor to the SM thresholds or EF slopes, expressed as the Pearson correlation in a multiple linear regression (SM thresholds (or EF slopes)= $b_0 + b_1 \times$ MAP + $b_2 \times$ Clay fraction + $b_3 \times$ VPD + $b_4 \times$ radiation + $b_5 \times$ wind + ε). ε represented other drivers that were not considered but might contribute to the variability of SM thresholds or EF slopes. The algorithm was implemented with the 'relaimpo' package in R (Grömping, 2006), which is based on variance decomposition for multiple linear regression

models. The 'relaimpo' package provides six different methods for analyzing the relative importance of each regressor in linear regression. We used 'LMG' to quantify the contribution of different correlated regressors in a multiple linear regression (Huang *et al.*, 2018). The LMG method estimates the relative importance (RI) of each variable by decomposing the sum of squares into non-negative contributions shared by each variable, and the LMG values were obtained by averaging the sequential sum of squares (r^2) for all possible orders. Finally, all RI values were normalized (divided by r^2) to sum to 1. We also repeated this analysis using the available energy (AE, the difference between net radiation and soil heat flux) instead of the incoming shortwave radiation to evaluate the relative role of AE.

3. Results

3.1 Surface energy partitioning characteristics and critical SM threshold of plant stress

EF behavior during all dry-downs within each vegetation type is plotted together in Figure 2. The general behavior is in line with that shown in Figure 1. Temperate grasslands and Mediterranean savannas showed stronger EF–SM coupling (greater slope) at low soil moisture values than boreal and temperate forests. The available energy is increasingly partitioned towards sensible heat flux with decreasing SM during the water-limited regime.

The surface SM thresholds (using SM_1) is highly correlated with the SM thresholds observed in deeper soil layers (using SM_2 and SM_3) (Fig. S4). As surface SM measurements are available at all sites, we focused on surface SM thresholds. Across all sites, we found that the critical SM threshold in Europe is 16.5 ± 7.5% (median ± SD, Fig. 3a). Temperate grasslands (27.0 ± 10.6%) had higher SM thresholds than temperate forests (16.5 ± 5.5%) and Mediterranean savannas (13.0 ± 1.6%, Fig. 3c). We also found that the soil matric potential threshold in savannas (−1.22 ± 0.21 MPa) is more negative than in forests (−0.64 ± 0.45 MPa) and grasslands (−0.37 ± 0.49 MPa, Fig. 3c). Overall, we estimated that the critical soil matric potential threshold across all sites in Europe is −0.71 ± 0.46 MPa (Fig. 3b).

The sensitivities (slopes) of EF to SM, time spent in water-limited stage, and the peak EFs are different among vegetation types (Fig. 4). Across all sites, EF decreased by 0.03 per 1% SM decrease (Fig. 4a). Savannas showed a higher sensitivity of EF to SM (slope 0.05 ± 0.02) than forests (slope 0.03 ± 0.02). We further found that the time spent in water-limited stage in savannas (82.9 ± 9.7% of all dry-down durations) was nearly two times as long as in forests (44.0 ± 24.1%); across all European sites, it was about 48.3 ± 27.0% of the dry-down period duration (Fig. 4b). However, the peak EF in energy-limited stage in forests (0.5 ± 0.1) tended to be higher than in savannas (0.4 ± 0.1, Fig. 4c).

3.2 Covariance between daily VPD and GPP during SM dry-down

As an alternative to the EF-SM relationships, the change in the sign of the covariance between daily GPP and VPD during dry-down was used to detect the critical SM threshold. To explore the dynamics of the VPD-GPP relationships during dry-down, we first illustrated the changes in the covariance of daily GPP and VPD during a long soil moisture dry-down at CH-Cha (grassland, Figs.5a, b), as well as the coincident changes in surface energy partitioning–SM relationship (Fig. 5c). Both the original data and moving average data found that daily GPP first increases but then decreases during the dry-down while daily VPD increases steadily (Fig. 5a). The sign of covariance between daily VPD and GPP changed from positive into negative around a SM threshold of 35% for this example (Fig. 5b). The positive covariances suggested that positive radiation effects (VPD-radiation coupling) on GPP are stronger while negative covariances showed that SM limiting effects on GPP are stronger (VPD-SM coupling). The EF-SM relationship showed that the EF values remain relatively high (about 0.75) at high SM (35-55%); however, under low SM (<35%), EF and SM were positively related in the interval during which reduced SM lowers EF (Fig. 5c). These observations are consistent with the notion that the ecosystem shifted from an energy-limited regime to a water-limited regime during this dry-down such that the sign of covariance between daily VPD and GPP was related to surface energy partitioning. Another example in a forest site, DE-Hzd, yielded similar results (Fig. S5).

We also examined the covariance between daily VPD and GPP for all soil dry-downs (Fig. 6). All covariances consistently changed their signs from positive to negative during the dry-down (Fig. 6a). We found that the median values of covariances across all dry-downs revealed that the breakpoint often occurs around the 4th moving window (the covariance is calculated using 9-day moving window, e.g., 1-9 days; 2-10 days; 3-11 days…). The changed covariance signs are also found in different vegetation types consistently (Figs. 6b-d). The timing of the breakpoint in forests (5th moving window, Fig. 6b) is larger than in grasslands (3rd moving window, Fig. 6c) and savannas (2nd moving window, Fig. 6d), suggesting that it takes longer for the VPD-GPP covariance sign to change from positive to negative in forests compared to grasslands and savannas. As the savanna sites have Mediterranean climate and the peak growing season is mainly in spring (El-Madany *et al.*, 2020, Luo *et al.*, 2018, Luo *et al.*, 2020), we performed the same analysis using both spring and summer and obtained similar results that the breakpoint in savannas is reached in shorter time than in forests (Fig. S6).

Combining the SM data for each dry-down (Figs. 6e-h), we then quantified the critical SM thresholds when the VPD-GPP covariance sign change at each site. We found that the θ_{crit} estimated from the new covariance method match well with the EF-SM method (r=0.86, Figs. 6i-j). Compared with the θ_{crit} estimated from the EF-SM method, our results showed that the VPD-GPP covariance method has potential to detect the critical moisture thresholds, although the absolute magnitude of SM thresholds estimated from covariance method are a bit higher than that of EF-SM methods (Figs. 6i-j).

3.3 Drivers of the spatial variability of SM thresholds and EF slopes

The multiple linear regression model showed that the five factors studied (mean annual precipitation, clay fraction, summer VPD, incoming shortwave radiation and wind speed) can explain 74% and 65% of the spatial variability of SM thresholds (Fig. 7a) and EF sensitivities (Fig. 7b), respectively. However, the dominant predictors of the spatial variability of SM thresholds and reduction rates of EF were different. For the spatial variability of SM

thresholds, soil texture was the most important factor, and its relative importance was 76% comparing with the other four factors (Fig. 7a), and clay fraction alone explained 65% of the variability across all sites. For the spatial variability of reduction rates of EF, climate factors, such as incoming shortwave radiation and VPD, were the major drivers, with relative importance up to 53% and 26%, respectively (Fig. 7b). The same analysis using the available energy (AE, the difference between net radiation and soil heat flux) instead of the incoming shortwave radiation obtained similar results (Fig. S7). AE played an important role in determining both the spatial variability of θ_{crit} (17%) and EF sensitivities (52%, Fig. S7).

4. Discussion

Current water stress indicators typically hinge on the accuracy of evapotranspiration data, a flux that is very difficult to measure globally and is often estimated with assumptions, thus leading to high degrees of uncertainty (Wang & Dickinson, 2012). To our knowledge, we demonstrate for the first time that the covariance between daily VPD and GPP changes its sign from positive to negative during SM dry-downs as ecosystems transition from energy-limited regimes to water-limited regimes. Our results suggest that the sign of covariance between daily VPD and GPP can capture shifts in the surface energy partitioning characteristics and therefore has potential to be a new indicator of ecosystem water stress. For global remote sensing data products, it becomes possible to have reasonable GPP products, e.g., based Near-Infrared Reflectance of vegetation (NIR_V) (Badgley *et al.*, 2017), normalized difference vegetation index (NDVI) (Myneni *et al.*, 1997), enhanced vegetation index (EVI) (Huete *et al.*, 2002) and daily FLUXCOM data (Jung *et al.*, 2017, Tramontana *et al.*, 2016), and VPD is computed from directly observed temperature and relative humidity, whereas global evapotranspiration products differ between datasets and are arguably more uncertain (Badgley *et al.*, 2015, Bai & Liu, 2018). Our covariance method provides a new option and an independent tool to quantify the critical SM threshold and detect surface energy partitioning characteristics over large regions, which we hope will be helpful to uncover the SM thresholds of plant water stress at regional and global scales. One advantage of the

covariance indicator is that, from a remote sensing perspective, spatially resolved VPD and GPP products have much lower levels of uncertainty than evapotranspiration products. Another is that the type of stress is directly related to GPP, i.e., carbon uptake, and not only indicative for stomatal conductance and transpiration.

Although the critical SM thresholds estimated from VPD-GPP covariance method match well with the EF-SM method, we found that the absolute magnitude of SM thresholds estimated from the VPD-GPP covariance method are a bit higher than the EF-SM method (Figs. 6i-j), which may result from two reasons. First, the covariance method calculated the covariance and mean SM values using nine-day moving windows. The average values of SM across the window could lead to the difference of SM thresholds between the VPD-GPP covariance method and EF-SM method. Second, the eddy covariance evapotranspiration analysis measures not only plant transpiration but also soil evaporation (though it is often small) (Stoy *et al.*, 2019), which may also contribute to the differences found between approaches. To get a more plant-related estimate of the critical SM threshold, the response of plant functioning (GPP and transpiration) with atmospheric stress (VPD) under given soil moisture conditions needs to be taken into account.

The timing when the sign of the covariance between VPD and GPP changes from positive to negative varies across vegetation types. Forests need more time for the sign of this relationship to change after rain events than grasslands and savannas, showing that there is a longer time during which VPD-radiation coupling is stronger than VPD-SM coupling in forests compared to grasslands and savannas during SM dry-downs. The water storage in soil and plants after rainfall in forests can be larger than in grasslands because forests have deeper roots and access to moisture in deeper soils (Chapin III *et al.*, 2011, Fan *et al.*, 2017). Forests often have stronger resistance to drought than grasslands and savannas (Konings & Gentine, 2017, Martínez-Vilalta & Garcia-Forner, 2017, Teuling *et al.*, 2010), thus GPP rates are maintained for a longer time after rainfall in forests.

The surface energy partitioning-SM relationship showed that grasslands and savannas had stronger EF–SM coupling (slope) at low soil moisture values than that of forests (Figs. 2

and 4a). Grasslands have shallow roots and are more sensitive to SM decrease, leading to abrupt drought, while forests have deep roots, access to deep soil water, and less sensitive to surface soil moisture changes. The high sensitivity of EF to SM in water-limited periods in grasslands and savannas will accelerate soil moisture depletion and quickly lead to large water constraints on photosynthesis (El-Madany *et al.*, 2020, Luo *et al.*, 2018, Luo *et al.*, 2020). The low sensitivity of EF to SM in forests is in line with our findings from covariance analysis that showed it takes longer for the VPD-GPP covariance sign to change from positive to negative in forests compared to grasslands and savannas, further supported the strong resistance of forests to drought (Konings & Gentine, 2017, Teuling *et al.*, 2010). We also found that incoming shortwave radiation and VPD are the major drivers in determining the spatial variability of EF sensitivity to SM, indicating that high radiation and VPD will increase the sensitivity of EF to SM in water-limited stage. This will likely cause EF sensitivity to increase in the future because increased exposure of plants to higher VPD from warming and drier continental relative humidity is inevitable and widespread in future (Byrne & O'Gorman, 2018, Novick *et al.*, 2016).

Consistent with previous findings from satellite observations in Africa (Feldman et al., 2019), our results showed that savannas spend more time in the water-limited regime, but we found that forests also spend almost 50% of the time in the water-limited regime, suggesting that European forest ecosystems are exposed to drought. This time fraction spent in the water-limited regime may further increase in future with anthropogenic warming (Naumann *et al.*, 2021), leading to greater drought damages in Europe. We also found that grasslands spend more than 70% of the time in the energy-limited regime because these grassland sites are mainly located in the northern Europe, which are limited by energy due to the high latitudes or altitudes. Under energy-limited stage, the peak EF in grasslands was up to 0.79 (Fig. 4c), indicating that grasslands allocate more energy for evaporative cooling, which suppresses surface heating (Teuling *et al.*, 2010).

Across all sites in Europe, our results showed that the critical SM threshold is 16.5% (Fig. 5), which is slightly higher than the value found in Africa (14%) using a different method

(Feldman *et al.*, 2019) and an oak–grass savanna (15%) and an annual grassland (15%) in US (Baldocchi *et al.*, 2004). At the European sites, we found that soil texture is the most important determining factor in controlling the spatial variability of SM thresholds (Fig. 7a), which is in line with previous findings in Africa (Feldman *et al.*, 2019) and the US (Akbar *et al.*, 2018), based on satellite data. We also converted the SM thresholds into soil matric potentials, and found that the soil matric potential threshold in Europe is about −0.71 MPa. The soil matric potential threshold in savannas is more negative than in forests and grasslands. When we focused on the forest sites in Europe, we found that the soil matric potential threshold is −0.64 MPa, which is very close from the -0.66 MPa value found by Granier *et al.* (2007) across six forest ecosystems. We noted that the EF-SM relationship can be affected by other factors, such as radiation and albedo (Haghighi *et al.*, 2018). While several other factors limit evapotranspiration besides soil moisture and the linear dependency is a simple approximation, recent studies have highlighted that this EF-SM framework provides a good first-order representation of regimes of land–atmosphere coupling, both in models and observations (e.g., Koster *et al.* (2004a); Koster *et al.* (2004b); Seneviratne *et al.* (2006); Teuling *et al.* (2006)). Here we provided a comprehensive analysis across representative European ecosystems.

5. Conclusions

Using a new database of flux tower observations across Europe, this study uncovered the critical SM threshold and surface energy partitioning characteristics by evaluating EF-SM relationships and examining the joint variability of daily VPD and GPP during SM dry-downs. We carefully studied SM dry-downs to understand how ecosystems transition from energy-limited regimes to water-limited regimes. EF-SM relationships quantified the critical SM and soil matric potential thresholds in Europe are 16.5% and −0.7 MPa, respectively. Surface energy partitioning characteristics varied among different vegetation types; EF in savannas had the highest sensitivities to SM in water-limited stage while it was the lowest in forests. We found the sign of covariance between daily VPD and GPP changed after a longer period

in forests than in grasslands and savannas. The critical SM thresholds estimated from the VPD-GPP covariance method match well with that of EF-SM method, suggesting that this sign of VPD-GPP covariance can be used to detect the SM threshold. We further found that soil texture dominates the spatial variability of SM thresholds while incoming shortwave radiation and VPD are the major drivers in determining the spatial pattern of EF sensitivities. The revealed critical SM threshold and its drivers across diverse biomes and climates in Europe will be beneficial to improve climate models with parametric representations of drought stress. Our results highlighted, for the first time, the important role of the sign change of covariance between daily VPD and GPP in monitoring the surface energy partitioning characteristics and quantifying the critical SM threshold, which opens its generalized application using daily GPP estimates and VPD, e.g., from remote sensing data. The new covariance method demonstrated here provides a new option and an independent tool to quantify critical SM threshold and surface energy partitioning, which can help solve the current challenge in uncovering the SM threshold of plant water stress at regional and global scales.

Acknowledgements

We would like to thank the ICOS Infrastructure for support in collecting and curating the flux tower data. This work was financially supported by the European Research Council Synergy project SyG-2013-610028 IMBALANCE-P and the ANR CLAND Convergence Institute. MG acknowledges funding by Swiss National Science Foundation project ICOS-CH Phase 2 20FI20_173691. AK and CM acknowledge funding by the Deutsche Forschungsgemeinschaft (INST 186/1118-1 FUGG). IM thanks ICOS-Finland and ACCC Flagship funded by the Academy of Finland grant number 337549. AV was supported by Russian Science Foundation (project 21-14-00209).

Conflict of interest

The authors declare no competing interests.

Data availability

The data that support the findings of this study are openly available in ICOS at (https://doi.org/10.18160/YVR0-4898).

References

Akbar R, Gianotti DJS, Mccoll KA, Haghighi E, Salvucci GD, Entekhabi D (2018) Estimation of landscape soil water losses from satellite observations of soil moisture. Journal of Hydrometeorology, **19**, 871-889.

Badgley G, Field CB, Berry JA (2017) Canopy near-infrared reflectance and terrestrial photosynthesis. Science advances, **3**, e1602244.

Badgley G, Fisher JB, Jiménez C, Tu KP, Vinukollu R (2015) On uncertainty in global terrestrial evapotranspiration estimates from choice of input forcing datasets. Journal of Hydrometeorology, **16**, 1449-1455.

Bai P, Liu X (2018) Intercomparison and evaluation of three global high-resolution evapotranspiration products across China. Journal of hydrology, **566**, 743-755.

Baldocchi DD, Xu L, Kiang N (2004) How plant functional-type, weather, seasonal drought, and soil physical properties alter water and energy fluxes of an oak–grass savanna and an annual grassland. Agricultural and Forest Meteorology, **123**, 13-39.

Bastos A, Ciais P, Friedlingstein P *et al.* (2020a) Direct and seasonal legacy effects of the 2018 heat wave and drought on European ecosystem productivity. Science advances, **6**, eaba2724.

Bastos A, Fu Z, Ciais P *et al.* (2020b) Impacts of extreme summers on European ecosystems: a comparative analysis of 2003, 2010 and 2018. Philosophical Transactions of the Royal Society B, **375**, 20190507.

Baty F, Ritz C, Charles S, Brutsche M, Flandrois J-P, Delignette-Muller M-L (2015) A toolbox for nonlinear regression in R: the package nlstools. Journal of statistical software, **66**, 1-21.

Betts AK (2004) Understanding hydrometeorology using global models. Bulletin of the American Meteorological Society, **85**, 1673-1688.

Budyko MI (1974) *Climate and life*, Academic press.

Byrne MP, O'gorman PA (2018) Trends in continental temperature and humidity directly linked to ocean warming. Proceedings of the National Academy of Sciences, **115**, 4863-4868.

Centre DTIET (2019) Drought-2018 ecosystem eddy covariance flux product in FLUXNET-Archive format - release 2019-1. ICOS Carbon Portal. (doi:10.18160/PZDK-EF78).

Chapin Iii FS, Matson PA, Vitousek P (2011) *Principles of terrestrial ecosystem ecology*, Springer Science & Business Media.

Dirmeyer PA, Koster RD, Guo Z (2006) Do global models properly represent the feedback between land and atmosphere? Journal of Hydrometeorology, **7**, 1177-1198.

El-Madany TS, Carrara A, Martín MP *et al.* (2020) Drought and heatwave impacts on semi-arid ecosystems' carbon fluxes along a precipitation gradient. Philosophical Transactions of the Royal Society B, **375**, 20190519.

Fan Y, Miguez-Macho G, Jobbágy EG, Jackson RB, Otero-Casal C (2017) Hydrologic regulation of plant rooting depth. Proceedings of the National Academy of Sciences, **114**, 10572-10577.

Feldman AF, Gianotti DJS, Konings AG, Mccoll KA, Akbar R, Salvucci GD, Entekhabi D (2018) Moisture pulse-reserve in the soil-plant continuum observed across biomes. Nature plants, **4**, 1026-1033.

Feldman AF, Short Gianotti DJ, Trigo IF, Salvucci GD, Entekhabi D (2019) Satellite-based assessment of land surface energy partitioning–soil moisture relationships and effects of confounding variables. Water Resources Research, **55**, 10657-10677.

Feldman AF, Short Gianotti DJ, Trigo IF, Salvucci GD, Entekhabi D (2020) Land-Atmosphere Drivers of Landscape-Scale Plant Water Content Loss. Geophysical Research Letters, **47**, e2020GL090331.

Fu Z, Ciais P, Bastos A *et al.* (2020) Sensitivity of gross primary productivity to climatic drivers during the summer drought of 2018 in Europe. Philos Trans R Soc Lond B Biol Sci, **375**, 20190747.

Gentine P, Green JK, Guérin M, Humphrey V, Seneviratne SI, Zhang Y, Zhou S (2019) Coupling between the terrestrial carbon and water cycles—a review. Environmental Research Letters, **14**, 083003.

Gourlez De La Motte L, Beauclaire Q, Heinesch B *et al.* (2020) Non-stomatal processes reduce gross primary productivity in temperate forest ecosystems during severe edaphic drought. Philosophical Transactions of the Royal Society B, **375**, 20190527.

Granier A, Reichstein M, Bréda N *et al.* (2007) Evidence for soil water control on carbon and water dynamics in European forests during the extremely dry year: 2003. Agricultural and Forest Meteorology, **143**, 123-145.

Green JK, Seneviratne SI, Berg AM, Findell KL, Hagemann S, Lawrence DM, Gentine P (2019) Large influence of soil moisture on long-term terrestrial carbon uptake. Nature, **565**, 476-479.

Grömping U (2006) Relative importance for linear regression in R: the package relaimpo. Journal of statistical software, **17**, 1-27.

Grossiord C, Buckley TN, Cernusak LA *et al.* (2020) Plant responses to rising vapor pressure deficit. New Phytologist, **226**, 1550-1566.

Haghighi E, Short Gianotti DJ, Akbar R, Salvucci GD, Entekhabi D (2018) Soil and atmospheric controls on the land surface energy balance: A generalized framework for distinguishing moisture-limited and energy-limited evaporation regimes. Water Resources Research, **54**, 1831-1851.

Huang K, Xia J, Wang Y *et al.* (2018) Enhanced peak growth of global vegetation and its key mechanisms. Nat Ecol Evol, **2**, 1897-1905.

Huete A, Didan K, Miura T, Rodriguez EP, Gao X, Ferreira LG (2002) Overview of the radiometric and biophysical performance of the MODIS vegetation indices. Remote Sensing of Environment, **83**, 195-213.

Jung M, Reichstein M, Schwalm CR *et al.* (2017) Compensatory water effects link yearly global land CO2 sink changes to temperature. Nature, **541**, 516-520.

Kimm H, Guan K, Gentine P *et al.* (2020) Redefining droughts for the U.S. Corn Belt: The dominant role of atmospheric vapor pressure deficit over soil moisture in regulating stomatal behavior of Maize and Soybean. Agricultural and Forest Meteorology, **287**, 107930.

Konings AG, Gentine P (2017) Global variations in ecosystem-scale isohydricity. Global change biology, **23**, 891-905.

Koster R, Schubert S, Suarez M (2009) Analyzing the concurrence of meteorological droughts and warm periods, with implications for the determination of evaporative regime. Journal of Climate, **22**, 3331-3341.

Koster RD, Dirmeyer PA, Guo Z *et al.* (2004a) Regions of strong coupling between soil moisture and precipitation. Science, **305**, 1138-1140.

Koster RD, Suarez MJ, Liu P *et al.* (2004b) Realistic initialization of land surface states: Impacts on subseasonal forecast skill. Journal of Hydrometeorology, **5**, 1049-1063.

Luo Y, El-Madany TS, Filippa G *et al.* (2018) Using near-infrared-enabled digital repeat photography to track structural and physiological phenology in Mediterranean tree–grass ecosystems. Remote Sensing, **10**, 1293.

Luo Y, El-Madany T, Ma X *et al.* (2020) Nutrients and water availability constrain the seasonality of vegetation activity in a Mediterranean ecosystem. Global change biology, **26**, 4379-4400.

Marthews TR, Quesada CA, Galbraith DR, Malhi Y, Mullins CE, Hodnett MG, Dharssi I (2014) High-resolution hydraulic parameter maps for surface soils in tropical South America. Geoscientific Model Development, **7**, 711-723.

Martínez-Vilalta J, Garcia-Forner N (2017) Water potential regulation, stomatal behaviour and hydraulic transport under drought: deconstructing the iso/anisohydric concept. Plant, Cell & Environment, **40**, 962-976.

Mccoll KA, Wang W, Peng B *et al.* (2017) Global characterization of surface soil moisture drydowns. Geophysical Research Letters, **44**, 3682-3690.

Myneni RB, Ramakrishna R, Nemani R, Running SW (1997) Estimation of global leaf area index and absorbed PAR using radiative transfer models. IEEE Transactions on Geoscience and remote sensing, **35**, 1380-1393.

Naumann G, Cammalleri C, Mentaschi L, Feyen L (2021) Increased economic drought impacts in Europe with anthropogenic warming. Nature Climate Change, **11**, 485-491.

Novick KA, Ficklin DL, Stoy PC *et al.* (2016) The increasing importance of atmospheric demand for ecosystem water and carbon fluxes. Nature Climate Change, **6**, 1023.

Pastorello G, Trotta C, Canfora E *et al.* (2020) The FLUXNET2015 dataset and the ONEFlux processing pipeline for eddy covariance data. Scientific data, **7**, 1-27.

Pendergrass AG, Meehl GA, Pulwarty R *et al.* (2020) Flash droughts present a new challenge for subseasonal-to-seasonal prediction. Nature Climate Change, **10**, 191-199.

Reichstein M, Falge E, Baldocchi D *et al.* (2005) On the separation of net ecosystem exchange into assimilation and ecosystem respiration: review and improved algorithm. Global change biology, **11**, 1424-1439.

Santanello Jr JA, Dirmeyer PA, Ferguson CR *et al.* (2018) Land–atmosphere interactions: The LoCo perspective. Bulletin of the American Meteorological Society, **99**, 1253-1272.

Schwingshackl C, Hirschi M, Seneviratne SI (2017) Quantifying spatiotemporal variations of soil moisture control on surface energy balance and near-surface air temperature. Journal of Climate, **30**, 7105-7124.

Seneviratne SI, Corti T, Davin EL *et al.* (2010) Investigating soil moisture–climate interactions in a changing climate: A review. Earth-Science Reviews, **99**, 125-161.

Seneviratne SI, Lüthi D, Litschi M, Schär C (2006) Land–atmosphere coupling and climate change in Europe. Nature, **443**, 205.

Shellito PJ, Small EE, Livneh B (2018) Controls on surface soil drying rates observed by SMAP and simulated by the Noah land surface model. Hydrology and Earth System Sciences, **22**, 1649-1663.

668 Short Gianotti DJ, Rigden AJ, Salvucci GD, Entekhabi D (2019) Satellite and station
669 observations demonstrate water availability's effect on continental-scale evaporative
670 and photosynthetic land surface dynamics. Water Resources Research, **55**, 540-554.
671 Stoy PC, El-Madany TS, Fisher JB *et al.* (2019) Reviews and syntheses: Turning the
672 challenges of partitioning ecosystem evaporation and transpiration into opportunities.
673 Biogeosciences, **16**, 3747-3775.
674 Teuling A, Seneviratne SI, Williams C, Troch P (2006) Observed timescales of
675 evapotranspiration response to soil moisture. Geophysical Research Letters, **33**.
676 Teuling AJ, Seneviratne SI, Stöckli R *et al.* (2010) Contrasting response of European forest
677 and grassland energy exchange to heatwaves. Nature Geoscience, **3**, 722.
678 Tramontana G, Jung M, Schwalm CR *et al.* (2016) Predicting carbon dioxide and energy
679 fluxes across global FLUXNET sites with regression algorithms.
680 Wang K, Dickinson RE (2012) A review of global terrestrial evapotranspiration: Observation,
681 modeling, climatology, and climatic variability. Reviews of Geophysics, **50**.
682 Zscheischler J, Orth R, Seneviratne SI (2015) A submonthly database for detecting changes in
683 vegetation-atmosphere coupling. Geophysical Research Letters, **42**, 9816-9824.
684

Figure legends

Fig. 1 Schematic of the typical relationship between evaporative fraction (EF) and soil moisture (SM), as well as the changes in daily SM, gross primary production (GPP) and vapor pressure deficit (VPD) during soil moisture dry-down. We hypothesize that the covariance between daily VPD and GPP can be used to detect two regimes during dry-downs, i.e., one regime with energy limiting conditions (positive covariance) and one regime with water limiting conditions (negative covariance). "+" and "-" represent the positive and negative correlation, respectively. RAD: incoming shortwave radiation. During a SM dry-down, there is generally an initial period of GPP increase due to available SM after rainfall if the ecosystem is already water limited before the dry-down counting started.

Fig. 2 EF-SM relationships for different vegetation types. Bold lines indicate binned median values calculated in equal SM bins of 1% increments, while shading bounds the 25th and 75th percentiles of EF values within soil moisture bins. EF: evaporative fraction; SM: soil moisture.

Fig. 3 Probability density function of estimated critical soil moisture (SM) threshold (a) and soil matric potential threshold (b). Estimated SM threshold and soil matric potential threshold among different vegetation types (c). For each box plot, the middle line indicates the median; the box indicates the upper and lower quartiles and the whiskers indicate the 5th and 95th percentiles of the data. The numbers in brackets indicate the number of sites.

Fig. 4 The evaporative fraction (EF) sensitivity to soil moisture (SM) (a), time fraction spent in water-limited stage (b) and the peak EF (c) among different vegetation types in Europe. For each box plot, the middle line indicates the median; the box indicates the upper and lower quartiles and the whiskers indicate the 5th and 95th percentiles of the data. The numbers in brackets indicate the number of sites.

Fig. 5 Daily soil moisture (SM), gross primary production (GPP) and vapor pressure deficit (VPD) during a soil dry-down at CH-Cha (grassland, a). Covariance between daily VPD and GPP changes with moving windows (b), and evaporative fraction (EF) changes with SM during the dry-down (c). The unit of covariance is μmol CO_2 m^{-2} s^{-1} hPa. The color coding in panel (c) indicate the soil moisture values. Please note that the soil moisture scale is from high to low.

Fig. 6 Covariance between daily vapor pressure deficit (VPD) and gross primary production (GPP) across nine-day moving window changes with moving windows after rainfall during the dry-down (a-d). Mean soil moisture (SM) during moving window for each dry-down (e-h). Comparison between the critical SM thresholds estimated from the VPD-GPP covariance method and evaporative fraction (EF) method (i-j). Covariance and mean soil moisture were calculated using 9-day moving window (e.g., 1-9 days; 2-10 days; 3-11 days…). Each black line represents the covariance change at each dry-

722 down while the red line means the median value in equal bins of 1 day change (a-d). The shading
723 bounds the 25th and 75th percentile of the distribution of covariance within the bin (a-d). The units of
724 covariance is μmol CO_2 m^{-2} s^{-1} hPa.
725
726 **Fig. 7** Relative importance of mean annual precipitation (MAP), clay fraction, summer average vapor
727 pressure deficit (VPD), incoming shortwave radiation (RAD) and wind speed to the spatial variability
728 of soil moisture (SM) thresholds (a) and evaporative fraction (EF) slopes (b).

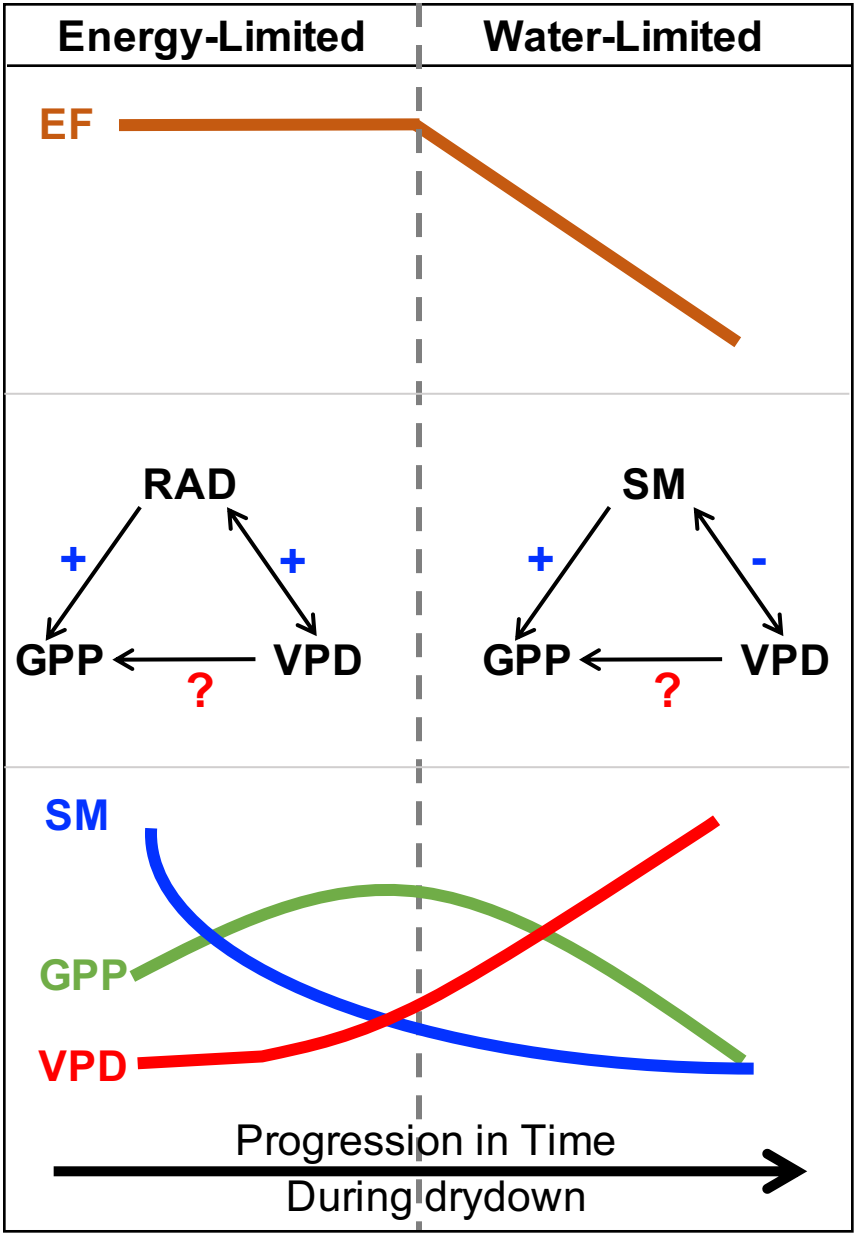
Energy-Limited
Water-Limited
EF
RAD
+
+
GPP
VPD
?
SM
+
-
GPP
VPD
?
SM
GPP
VPD
Progression in Time
During drydown

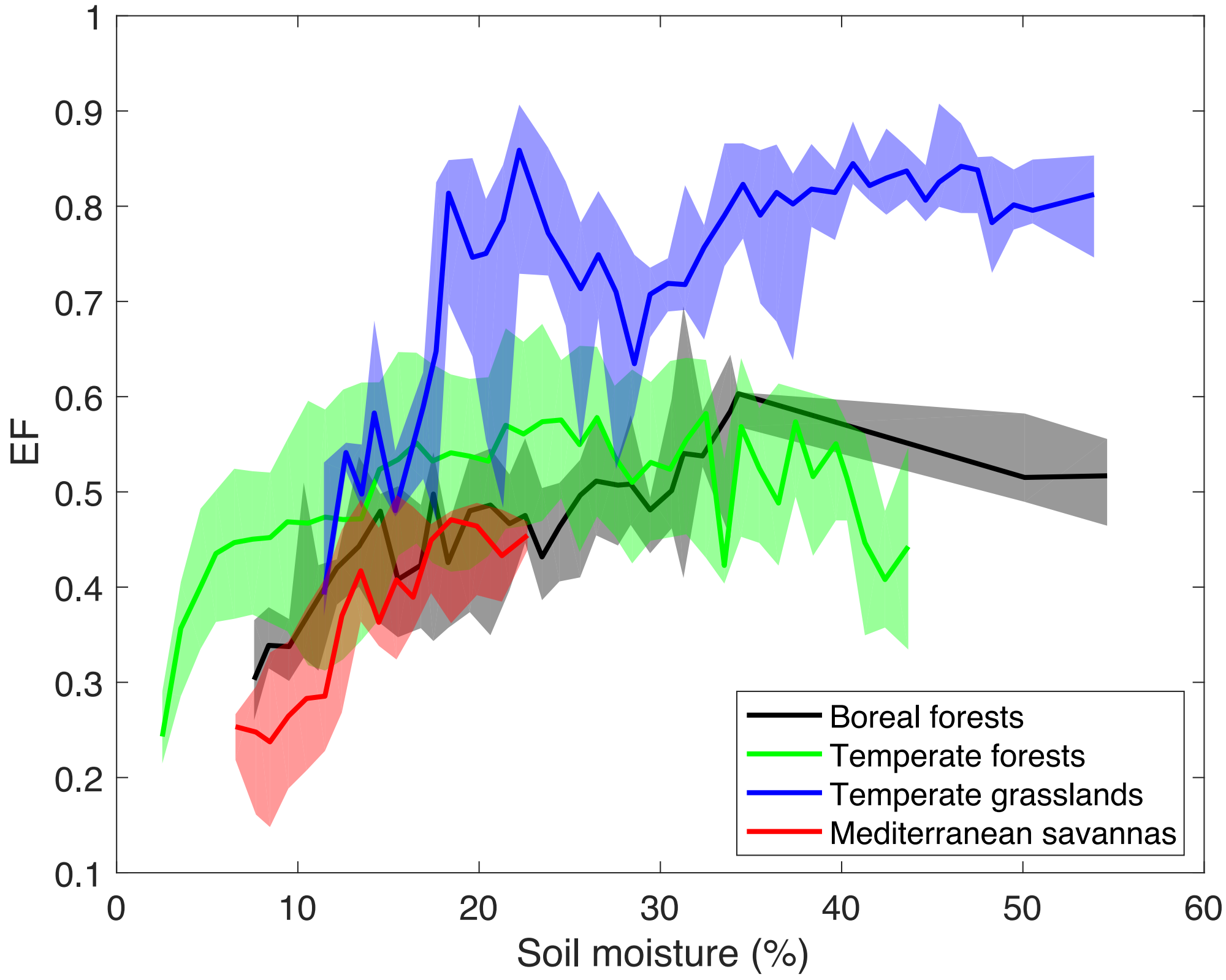
EF
Soil moisture (%)
1
0.9
0.8
0.7
0.6
0.5
0.4
0.3
0.2
0.1
0
10
20
30
40
50
60
Boreal forests
Temperate forests
Temperate grasslands
Mediterranean savannas

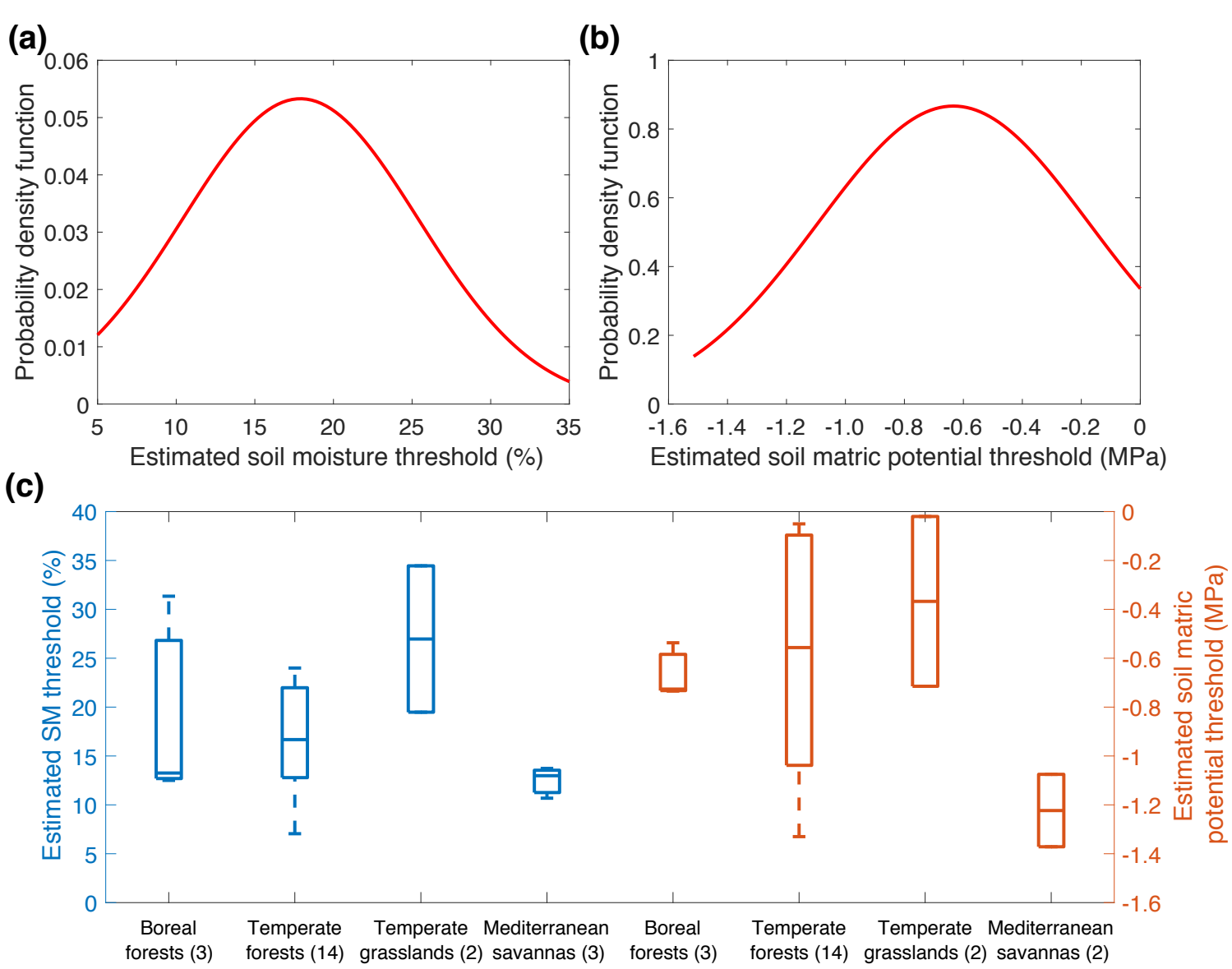
(a)
Probability density function
0.06
0.05
0.04
0.03
0.02
0.01
0
5
10
15
20
25
30
35
Estimated soil moisture threshold (%)
(b)
Probability density function
1
0.8
0.6
0.4
0.2
0
-1.6
-1.4
-1.2
-1.0
-0.8
-0.6
-0.4
-0.2
0
Estimated soil matric potential threshold (MPa)
(c)
Estimated SM threshold (%)
40
35
30
25
20
15
10
5
0
Estimated soil matric potential threshold (MPa)
0
-0.2
-0.4
-0.6
-0.8
-1
-1.2
-1.4
-1.6
Boreal forests (3)
Temperate forests (14)
Temperate grasslands (2)
Mediterranean savannas (3)
Boreal forests (3)
Temperate forests (14)
Temperate grasslands (2)
Mediterranean savannas (2)

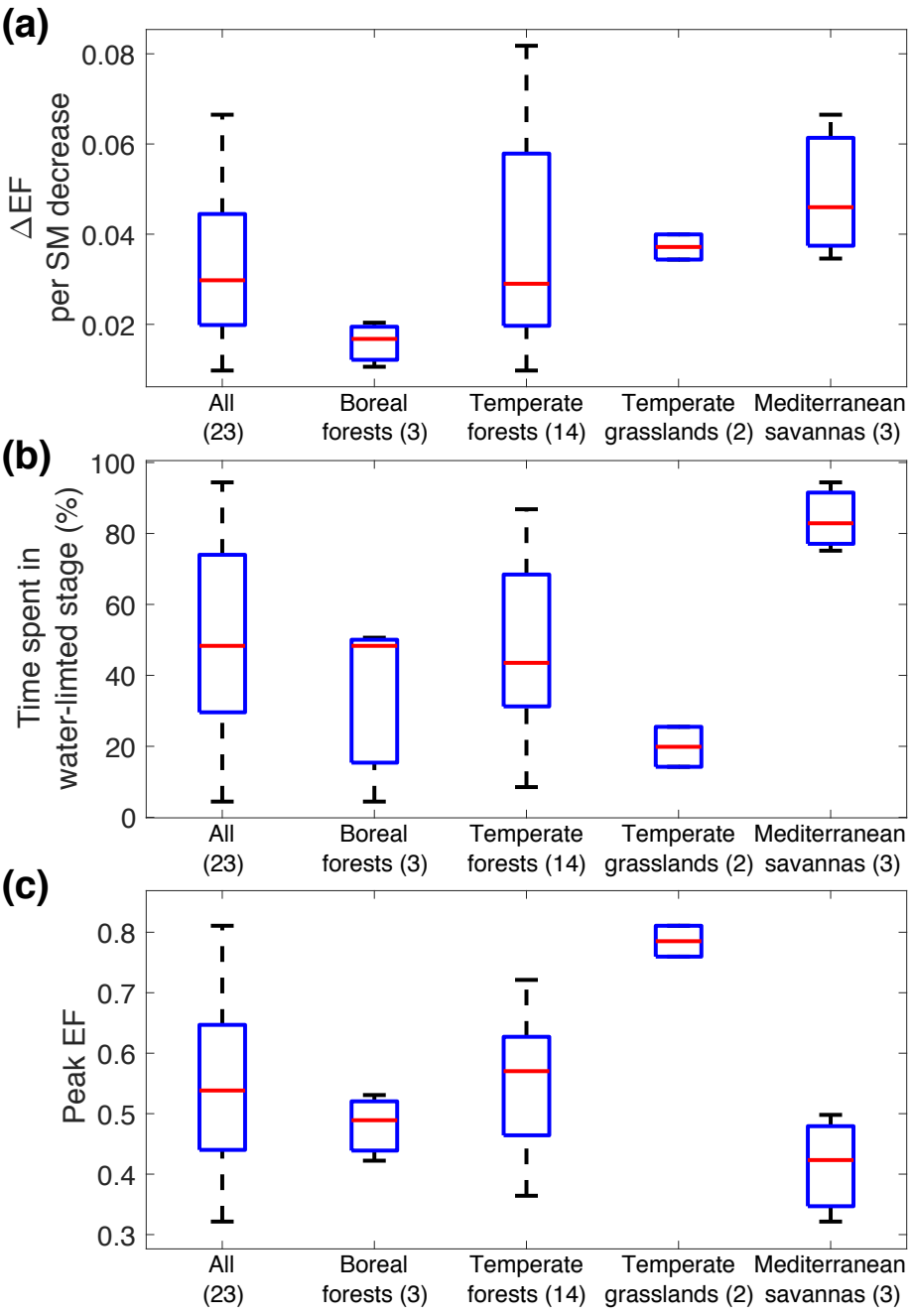
(a)
ΔEF
per SM decrease
0.08
0.06
0.04
0.02
All
(23)
Boreal
forests (3)
Temperate
forests (14)
Temperate
grasslands (2)
Mediterranean
savannas (3)
(b)
Time spent in
water-limted stage (%)
100
80
60
40
20
0
All
(23)
Boreal
forests (3)
Temperate
forests (14)
Temperate
grasslands (2)
Mediterranean
savannas (3)
(c)
Peak EF
0.8
0.7
0.6
0.5
0.4
0.3
All
(23)
Boreal
forests (3)
Temperate
forests (14)
Temperate
grasslands (2)
Mediterranean
savannas (3)

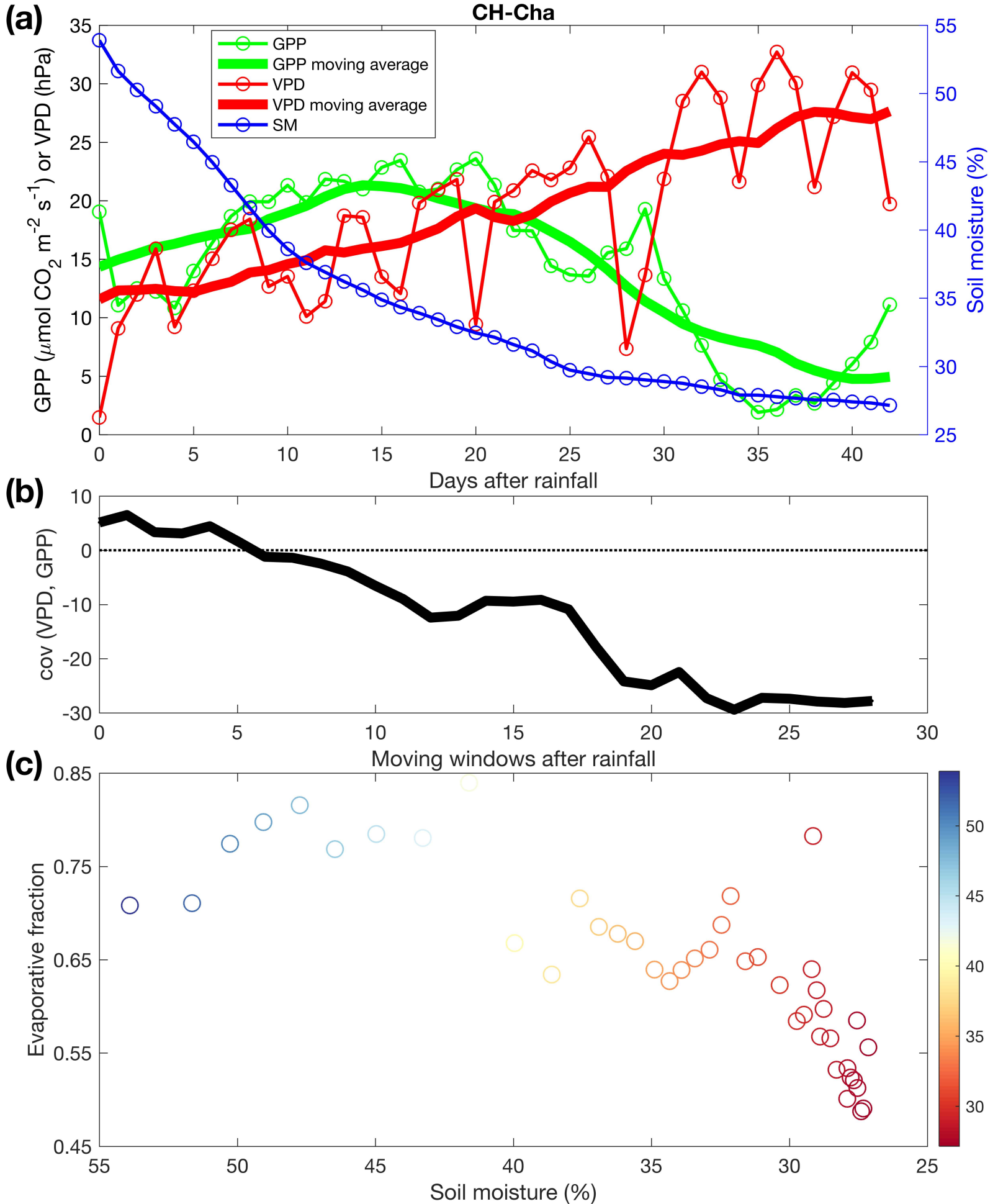
(a)
CH-Cha
GPP
GPP moving average
VPD
VPD moving average
SM
GPP (μmol CO2 m-2 s-1) or VPD (hPa)
Soil moisture (%)
Days after rainfall
(b)
cov (VPD, GPP)
Moving windows after rainfall
(c)
Evaporative fraction
Soil moisture (%)

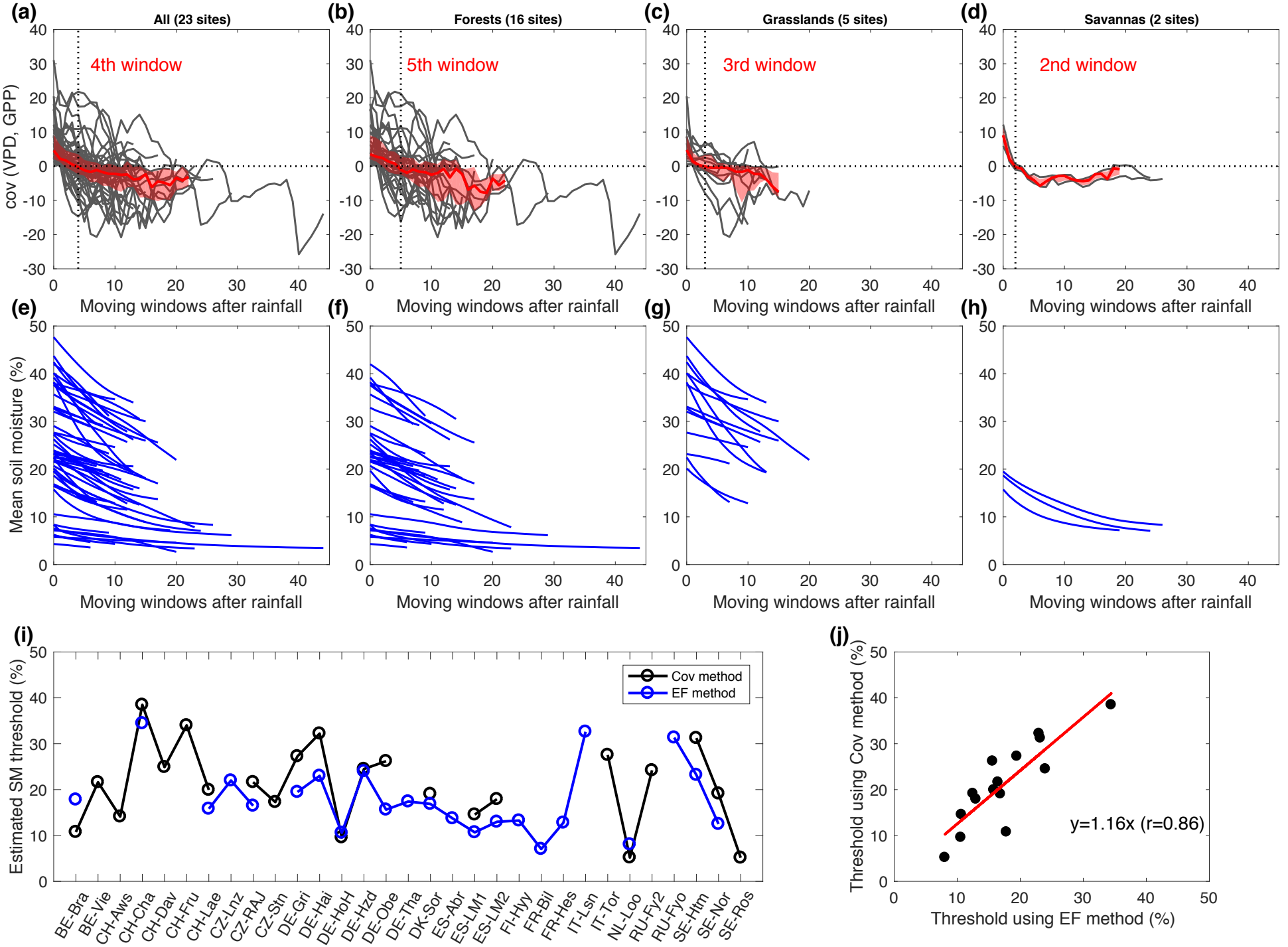
(a)
All (23 sites)
4th window
(b)
Forests (16 sites)
5th window
(c)
Grasslands (5 sites)
3rd window
(d)
Savannas (2 sites)
2nd window
cov (VPD, GPP)
Moving windows after rainfall
(e)
(f)
(g)
(h)
Mean soil moisture (%)
(i)
Estimated SM threshold (%)
Cov method
EF method
BE-Bra
BE-Vie
CH-Aws
CH-Cha
CH-Dav
CH-Fru
CH-Lae
CZ-Lnz
CZ-RAJ
CZ-Sth
DE-Gri
DE-Hai
DE-HoH
DE-Hzd
DE-Obe
DE-Tha
DK-Sor
ES-Abr
ES-LM1
ES-LM2
FI-Hyy
FR-Bil
FR-Hes
IT-Lsn
IT-Tor
NL-Loo
RU-Fy2
RU-Fyo
SE-Htm
SE-Nor
SE-Ros
(j)
Threshold using Cov method (%)
Threshold using EF method (%)
y=1.16x (r=0.86)

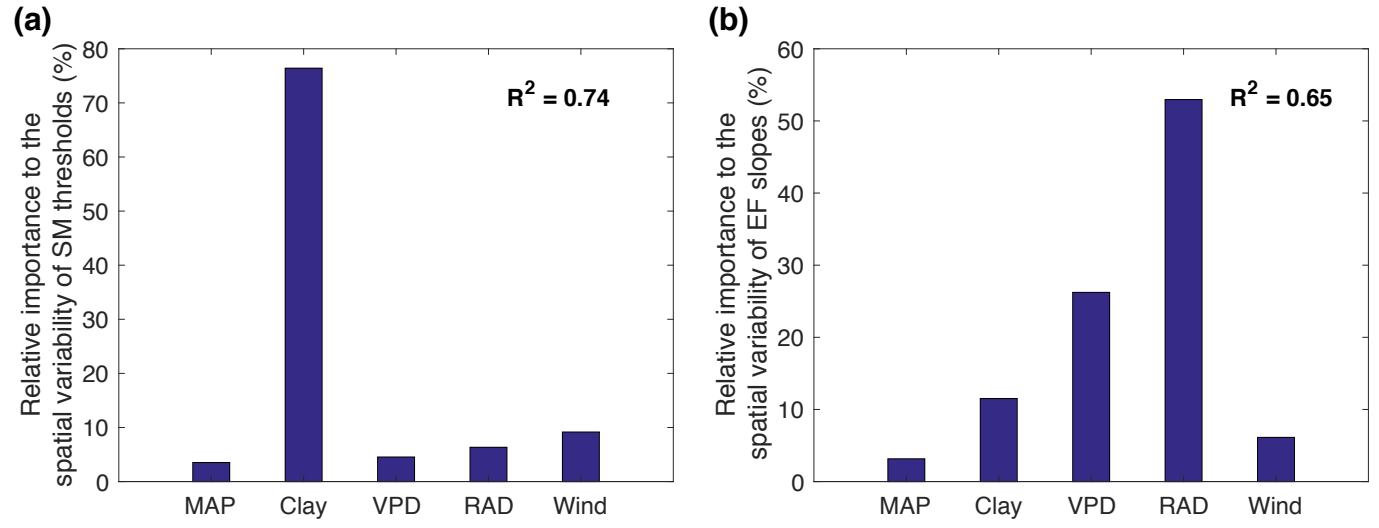
(a)
Relative importance to the spatial variability of SM thresholds (%)
80
70
60
50
40
30
20
10
0
R2 = 0.74
MAP
Clay
VPD
RAD
Wind
(b)
Relative importance to the spatial variability of EF slopes (%)
60
50
40
30
20
10
0
R2 = 0.65
MAP
Clay
VPD
RAD
Wind